

# PHENIX Highlights

Takao Sakaguchi (for the PHENIX Collaboration)<sup>1</sup>

*Brookhaven National Laboratory, Physics Department, Upton, NY 11973, USA*

---

## Abstract

PHENIX reports on electromagnetic and hadronic observables in large data sets of p+p, d+Au and Au+Au collisions at various cms energies. Initial state effects in cold nuclear matter are quantified by centrality dependent  $\pi^0$ ,  $\eta$ , reconstructed jets and  $\psi'$  measurements. Using the first run of the new EBIS ion source at RHIC, we report first results for particle flow ( $v_1$  and  $v_2$ ) and quarkonium production in U+U and Cu+Au collisions. Hot matter created in Au+Au is characterized using event-plane dependent HBT and dielectrons. Parton-medium interactions are investigated using high  $p_T$  single hadrons,  $\gamma$ -hadron correlations and heavy flavor decay electrons identified with the newly installed VTX detector.

---

## 1. Introduction

RHIC experiments have demonstrated that quark-gluon plasma (QGP) is created in Au+Au collisions. Subsequent experimental goals focus on characterizing the QGP, and exploring the phase transition and a possible critical point by varying the colliding nuclei and collision energy. We present the latest results from the PHENIX experiment at RHIC. The results are categorized according to time within the collision: initial state effects, hot matter dynamics, and parton-medium interactions.

## 2. The baseline for QGP properties

Initial state effects on the primordial hard scatterings which produce hard probes of the hot dense medium reflect parton distribution functions in nucleons and nuclei, as well as possible energy loss or bound state dissociation in cold matter. p+p collisions provide the baseline, while d+Au collisions reflect additional cold nuclear matter (CNM) effects arising from the presence of a nucleus in the collision. Direct photon spectra in d+Au collisions show little or no modification compared to expectations from p+p collisions, though an isospin effect is consistent with the data [1, 2]. On the other hand, hadronic probes display centrality-dependent CNM effects.

In Fig. 1, the nuclear modification factors ( $R_{dA}$ ) for  $\pi^0$ ,  $\eta$  and fully-reconstructed jets in d+Au collisions at  $\sqrt{s_{NN}}=200$  GeV are shown [3]. These three probes result from different analysis techniques, but show remarkable consistency. While a slight suppression is found in the most central collisions, there is significant enhancement at high  $p_T$  in the peripheral collisions; such

---

<sup>1</sup>A list of members of the PHENIX Collaboration and acknowledgements can be found at the end of this issue.

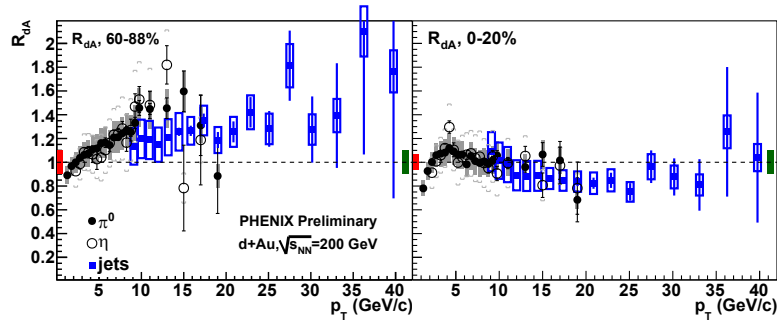


Figure 1: Nuclear modification factors ( $R_{dA}$ ) for  $\pi^0$ ,  $\eta$  and fully-reconstructed jets in d+Au collisions.

a feature is not predicted by available models. We note that centrality is determined in the data by the particle multiplicity in the beam-beam counter (BBC) at  $3.1 < |\eta| < 3.9$ , while the models use impact parameters. Therefore, the centrality classes between data and models may differ somewhat, particularly for events with high  $p_T$  hadrons or jets ( $p_T > 10$  GeV).

Quarkonia offer key probes of initial state effects. The high statistics 2008 data enable measurement of  $\psi'$  production as a function of collision centrality in d+Au at  $\sqrt{s_{NN}}=200$  GeV. The dielectron mass spectrum in the  $J/\psi$  and  $\psi'$  region is shown in Fig. 2 [3]. The ratio of  $\psi'/(J/\psi)$  is

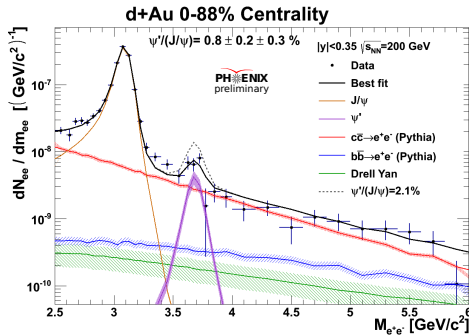


Figure 2:  $\psi'$  peak seen in dielectron mass spectra in minimum bias d+Au collisions.

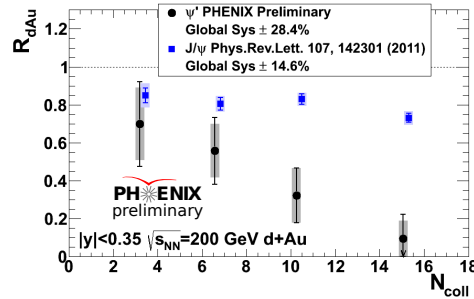


Figure 3:  $R_{dA}$  of  $\psi'$  and  $J/\psi$  in d+Au collisions as a function of centrality.  $\psi'$  is more suppressed than  $J/\psi$ .

$\sim 0.8\%$ , smaller than in p+p (2.1%). The centrality dependence of the ratio is shown in Fig. 3. The yield of  $J/\psi$  is somewhat suppressed in d+Au collisions compared to p+p, but  $\psi'$  is more heavily suppressed. The relative suppression at FNAL fixed target energy can be reasonably well explained by considering the time the precursor  $c\bar{c}$  state spends in the nucleus. However, this explanation completely fails at RHIC energy.

### 3. New collision systems for QGP characterization

In 2012, first data were taken with the EBIS ion source, providing new ion species at RHIC.

### 3.1. U+U collisions

Uranium is a highly deformed nucleus. Therefore, selecting collisions where two uranium nuclei are aligning with their long axes head-on (tip-tip) should access higher energy density at RHIC energy. PHENIX collected data in U+U collisions at  $\sqrt{s_{NN}}=193$  GeV. First results show that the Bjorken energy density for 0-2 % centrality (tip-tip enriched events) is  $\sim 30$  % higher than the most central Au+Au collisions at 200GeV [4]. The elliptic flow of identified charged pions and protons in U+U collisions are compared to that in Au+Au at 0-10 % centrality in Fig. 4 [5]. For pions in U+U,  $v_2$  is flatter with  $p_T$  for  $p_T < 1$  GeV, reminiscent of observations in Pb+Pb at

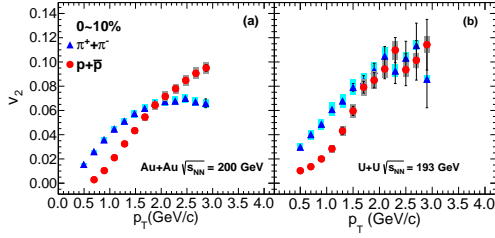


Figure 4: Elliptic flow of charged pions and protons in (a) Au+Au and (b) U+U collisions at 0-10 % centrality.

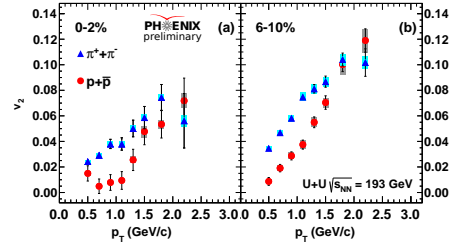


Figure 5: Elliptic flow of charged pions and protons in (a) 0-2 % and (b) 6-10 % centrality in U+U collisions.

LHC [6]. This can be interpreted as a consequence of very strong radial flow for higher energy density matter. The finer centrality classes shown in Fig. 5 show that this flattening is most pronounced in 0-2 %, where tip-tip events represent a larger fraction of the total, and is nearly nonexistent for 6-10 % centrality. It is intriguing to see this phenomenon at RHIC, as the energy density reached at LHC is  $\sim 3$  times higher than at RHIC.

### 3.2. Cu+Au collisions

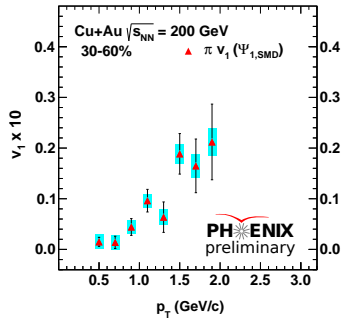


Figure 6:  $v_1$  of charged pions in Cu+Au collisions.

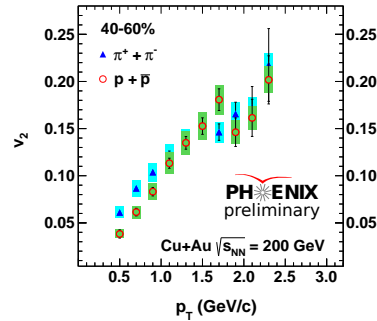


Figure 7:  $v_2$  of charged pions and protons in Cu+Au collisions.

In Cu+Au collisions, one can select events in which the Cu is fully contained within the Au nucleus. Furthermore, the pressure gradient developed should be asymmetric, resulting in an

intrinsic triangularity in the collective motion. This triangularity generates a  $v_3$  that is geometric, rather than fluctuation driven. PHENIX has already analyzed  $\sim 20\%$  of the 2012 Cu+Au data. The shower-max detector in the zero-degree calorimeters is used to determine the event plane (reaction plane  $\Psi_1$ ), allowing a measurement of  $v_1$ . We defined the Au-spectator going side as positive  $\Psi_1$ .

Fig. 6 and 7 show  $v_1$  and  $v_2$  for identified pions and protons. A sizable positive  $v_1$  is observed; the sign and magnitude of  $v_1$  differ from predictions of the the AMPT model (HIJING+parton cascade) [7], although AMPT describes symmetric collision systems very well.

Utilizing the muon arms at  $1.2 < |\eta| < 2.2$ , PHENIX measured  $J/\psi$  spectra in Cu+Au collisions via the di-muon decay channel. This allowed determination of  $J/\psi R_{AA}$  in Cu+Au, and comparison to the the  $J/\psi$  suppression observed in Cu+Cu and Au+Au collisions. The results and comparison are shown in Fig. 8 [8]. The suppression of the  $J/\psi$  yield as a function of  $N_{part}$

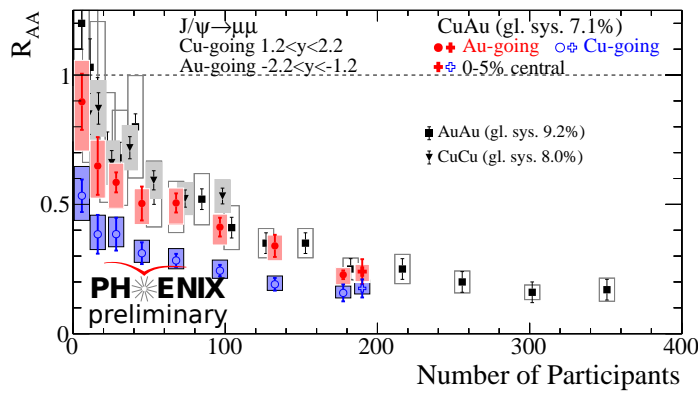


Figure 8:  $R_{AA}$  of  $J/\psi$  in Cu+Au, Cu+Cu and Au+Au collisions.

on the Au-going side fits well with the  $N_{part}$  dependence in Au+Au and Cu+Cu collisions. However, on the Cu-going side, the suppression is significantly stronger. The difference of the nuclear PDFs in Cu and Au nuclei partly explains this trend, but additional final state effects may need to be considered in order to understand the magnitude on the Cu-going side.

#### 4. Characterizing hot dense matter by new probes

Two boson correlations as pioneered by Hanbury-Brown and Twiss (colloquially known as HBT correlations in our field) provide information on the space-time evolution of the particle emission source. PHENIX has measured the angular dependence of HBT radii with respect to the (second order) event plane ( $R_s^2(\Delta\phi) = R_{s,0}^2 + 2 \times \Sigma R_{s,n}^2 \cos(n\Delta\phi)$ ). This analysis shows that the eccentricity, defined as  $\epsilon_{HBT} = 2R_{s,2}^2/R_{s,0}^2$ , obtained from the Kaon HBT correlations is consistent with the initial eccentricities. This implies early freezeout of kaons from the expanding hadronic phase late in the collision.

PHENIX studied the HBT radii with respect to the 3rd order event plane for the first time. Fig. 9 shows  $R_s$  and  $R_o$  for charged pions as a function of the emission angle with respect to the 2nd and 3rd order event plane in 0-10% in Au+Au collisions [9]. The average radii are 10 and 5

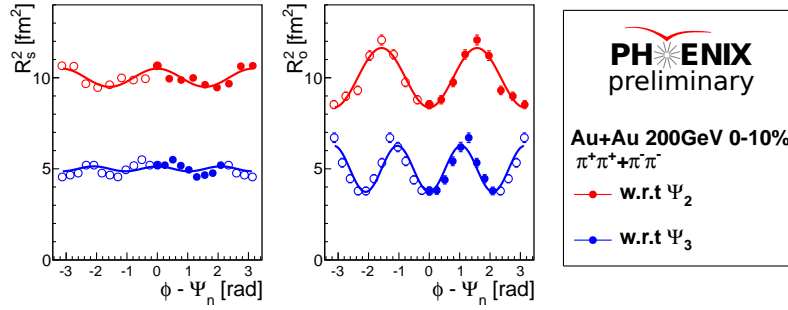


Figure 9: Angular dependence of HBT radii ( $R_s$  and  $R_o$ ) with respect to 2nd ( $\Psi_2$ ) and 3rd ( $\Psi_3$ ) order event plane in 0-10% Au+Au collision at  $\sqrt{s_{NN}}=200$  GeV.

for  $\Psi_2$  and  $\Psi_3$ , respectively. While  $R_s$  shows only a weak dependence on orientation with respect to the event plane,  $R_o$  indicates a clear temporal variation as a function of angle for both the  $\Psi_2$  and  $\Psi_3$  event planes. Moreover, the magnitude of the oscillation for  $\Psi_3$  is almost the same as  $\Psi_2$ . Since  $R_o$  includes the emission duration in addition to the spatial homogeneity length in the transverse direction, this measurement reflects the space-time evolution of ellipticity and triangularity of the collision system.

Turning to thermal radiation, we report on a unique and penetrating probe of thermodynamic quantities. Measuring thermal radiation gives access, for example, to the temperature of the hot dense medium produced in the collision. Using the Hadron Blind Detector (HBD) installed in 2010, PHENIX performed a new measurement of thermal di-electron radiation. In all bins from peripheral to semi-central, the new result is consistent with that from the 2004 data. The most central bin is still being analyzed. For further details, see [10].

## 5. Detailed study of energy loss of partons

### 5.1. $\gamma$ -h correlation

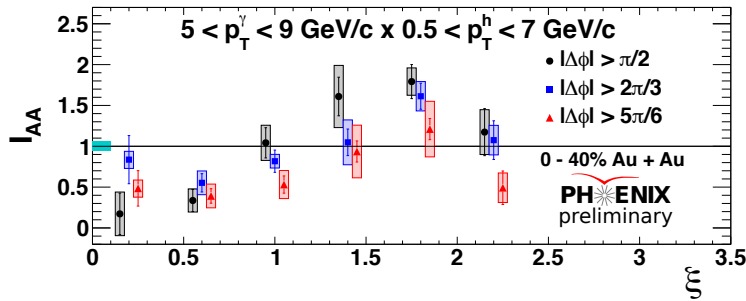


Figure 10: Ratio of per-trigger away-side hadron yield in 200 GeV Au+Au and p+p  $\gamma$ -hadron measurements as a function of  $\xi$ . The legend identifies the three different integrating angular ranges.

$\gamma$ -hadron correlations are often considered a "golden channel" to evaluate the energy loss of partons in the medium. Since direct photons reflect the momentum of the original scattered

partons, they tag the initial momentum of the scattered parton that traverses the medium. Consequently one can deduce the energy loss via  $\delta p_T = p_T(\gamma) - p_T(\text{hadrons})$ . PHENIX has measured the hadron yield opposing direct photons as a function of  $\xi(\equiv -\ln(z_T))$  for the 2007 and 2010 Au+Au data sets together. The results are shown in Fig. 10 [11]. As the angular range in which the away-side hadrons are integrated is increased from  $|\delta\phi| > 5\pi/6$  to  $|\delta\phi| > \pi/2$ , the per-trigger away-side yield increases compared to p+p collisions. The increase is in the larger  $\xi$  or small  $z_T$  region, implying that the softer away-side jet fragments are distributed over a wider angle than fragments carrying a large fraction of the jet energy. This is expected from medium-enhanced splitting, and is qualitatively consistent with the angular broadening observed in hadron-hadron correlations at RHIC and the jet shape broadening observed at LHC.

### 5.2. High $p_T \pi^0$ to determine fractional momentum shift

Using the large 2007 Au+Au data set at  $\sqrt{s_{NN}} = 200$  GeV and a new algorithm to correct for shower merging, PHENIX extended the  $p_T$  range of  $\pi^0$  spectra [12]. Fig. 11 compares  $\pi^0 R_{AA}$  in 200 GeV Au+Au collisions from RHIC and charged hadron  $R_{AA}$  measured in 2.76 TeV Pb+Pb at the LHC (ALICE experiment) [13]. For both centralities and over the entire  $p_T$  range shown, the two data sets are rather similar. However, this does not necessarily mean that the energy

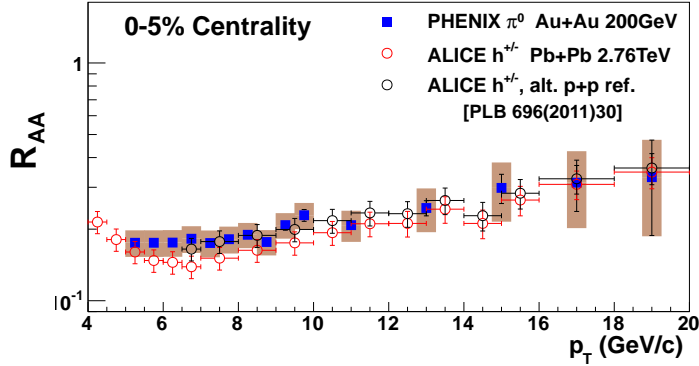


Figure 11: Comparison of  $R_{AA}$  of  $\pi^0$  from PHENIX at RHIC and charged hadrons from ALICE experiments at LHC. Two data sets from ALICE experiments correspond to two different p+p references.

loss of the partons is the same, as the spectral shapes differ. PHENIX determines the average fractional momentum shift ( $S_{loss}$ ) of high  $p_T \pi^0$  to estimate the average fractional energy loss of the initial parton.  $S_{loss}$  is defined as  $\delta p_T / p_T$ , where  $\delta p_T$  is the difference of the momentum in p+p collisions ( $p_{T,pp}$ ) and Au+Au ( $p_{T,AuAu}$ );  $p_T$  in the denominator is  $p_{T,pp}$ . The calculation method is schematically depicted in Fig. 12. First, the  $\pi^0$  cross-section in p+p ( $f(p_T)$ ) is scaled by  $T_{AA}$  corresponding to the centrality selection of the Au+Au data ( $g(p_T)$ ). Next, the scaled p+p cross-section ( $T_{AA}f(p_T)$ ) is fit with a power-law function ( $h(p_T)$ ). Third, a scaled p+p point closest in yield ( $p'_{T,pp}$ ) to the Au+Au point of interest ( $p_{T,AuAu}$ ) is shifted using the fit function as

$$T_{AA}f(p_{T,pp}) = h(p_{T,pp})/h(p'_{T,pp}) \times T_{AA}f(p'_{T,pp}), \quad (1)$$

where  $p_{T,pp}$  is chosen to satisfy the relation

$$T_{AA}f(p_{T,pp}) = g(p_{T,AuAu}). \quad (2)$$

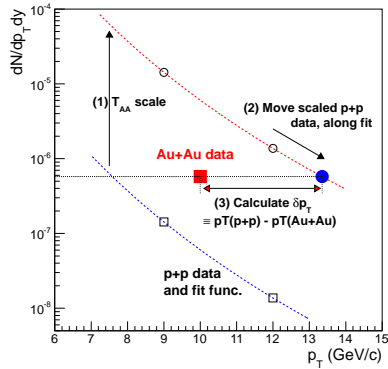


Figure 12: Demonstration of calculating the fractional momentum loss ( $S_{loss}$ ).

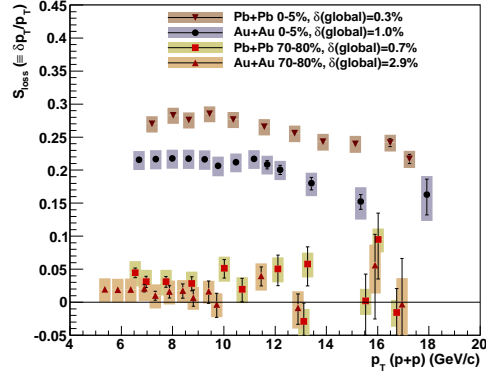


Figure 13:  $S_{loss}$  for PHENIX  $\pi^0$  and ALICE charged hadrons.

The  $\delta p_T$  is calculated as  $p_{T,pp} - p_{T,AuAu}$ . For obtaining  $S_{loss}$ , the  $\delta p_T$  is divided by the  $p_{T,pp}$ . We show the comparison of  $S_{loss}$  for PHENIX  $\pi^0$ 's in Au+Au and ALICE charged hadrons in Pb+Pb in Fig. 13. We took the corresponding Pb+Pb and p+p data for black points in Fig. 11 for calculating the  $S_{loss}$  for ALICE charged hadrons. The  $S_{loss}$  for the ALICE charged hadrons is found to be  $\sim 25\%$  higher than that for the PHENIX  $\pi^0$ 's. PHENIX has also measured  $S_{loss}$  in Au+Au at 39 and 62.4 GeV cms energy. The change in  $S_{loss}$  reaches approximately a factor of 4 from 200 GeV to 39 GeV [14, 15].

## 6. Heavy flavor electrons

The suppression of non-photonic electron yields was found to be nearly as large as that of  $\pi^0$ 's. The question has been whether the suppression arises from the suppression of charm and/or bottom quarks. Theoretical predictions about this differ greatly. Consequently, PHENIX constructed a micro vertex detector to separate electrons from charm and bottom decays. This detector, the VTX, consists of 2 layers each of strip-pixel and pixel silicon detectors. The measurement of the distance of closest approach (DCA) of electrons to the collision vertex allows separation according to the parent hadrons. Fig. 14 shows a DCA distribution measured in the VTX detector in p+p collisions. The distribution was deconvoluted to determine the relative contributions of the heavy flavor parent hadrons. Fig. 15 shows the ratio of electron yields from b-quarks, and b + c quarks for p+p collisions [8]. The points with large error bars are from  $K\pi$  correlation measurements [16]. Our new result is consistent with both the  $K\pi$  correlation analysis and with FONLL calculations. We also analyzed electrons in Au+Au collisions to obtain the  $R_{AA}$  for electrons from charm and bottom quarks [8]. The analysis assumed that the parent hadrons (e.g. D, B) follow the  $p_T$  distributions given by PYTHIA. The results demonstrate that the Au+Au data are inconsistent with these input assumptions unless there is also a large suppression of electrons from bottom across the measured  $p_T^e$  range. However, this large suppression implies a change in the parent hadron  $p_T$  distributions, which results in changes in the electron DCA distributions. We are actively working on evaluation of the uncertainties caused by this fact.

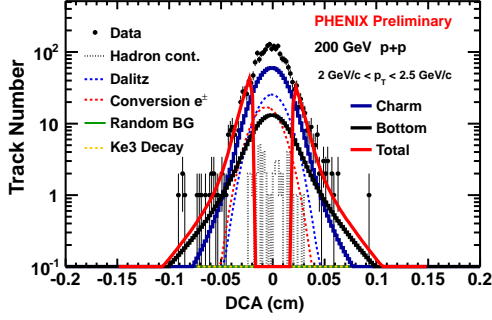


Figure 14: DCA distribution in p+p collisions for  $2 < p_T^e < 2.5 \text{ GeV}/c$ , and its deconvolution to contributions from parent hadrons.

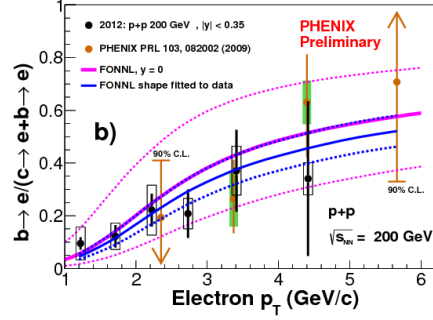


Figure 15: Ratio of electron yields from bottom quarks to bottom and charm quarks in p+p collisions.

## 7. Summary

PHENIX has reported new findings in collisions at various energies and species available at RHIC. There is a significant enhancement of high  $p_T$  hadrons and jets in the peripheral d+Au collisions. The yield of  $\psi'$  is more heavily suppressed than that of  $J/\psi$  in d+Au collisions. A strong radial flow is seen in tip-tip enriched 0-2% U+U collisions. A sizable positive  $v_1$  is observed in Cu+Au collisions. In the same system, the  $J/\psi$  yield measured in  $1.2 < |\eta| < 2.2$  as a function of  $N_{part}$  shows larger suppression in the Cu-going side than the Au-going side. The space-time evolution of the ellipticity and triangularity of the Au+Au collision system is observed in angular dependent HBT measurement. PHENIX has seen an angular broadening of the away-side soft particles in  $\gamma$ -h measurement, similar to h-h correlations and jet shape measurements from RHIC and LHC. The high  $p_T$  hadron spectra showed that the fractional momentum shift under the presence of hot dense matter is  $\sim 25\%$  higher at LHC compared to the RHIC top energy. Identification of electrons from bottom and charm quarks has been successful at RHIC using the VTX detector. The ratio of  $(b \rightarrow e)/(b, c \rightarrow e)$  for p+p collisions is consistent with the previous measurement and well described by a FONLL calculation.

## References

- [1] A. Adare *et al.* [PHENIX Collaboration], arXiv:1205.5533 [hep-ex].
- [2] A. Adare, *et al.* [PHENIX Collaboration], arXiv:1208.1234 [nucl-ex].
- [3] M. Wysocki [PHENIX Collaboration], these proceedings.
- [4] J. Mitchell [PHENIX Collaboration], these proceedings.
- [5] S. Huang [PHENIX Collaboration], these proceedings.
- [6] K. Safarik, [ALICE Collaboration], these proceedings.
- [7] Z. -W. Lin, C. M. Ko, B. -A. Li, B. Zhang and S. Pal, Phys. Rev. C **72**, 064901 (2005).
- [8] M. Rosati [PHENIX Collaboration], these proceedings.
- [9] T. Niida [PHENIX Collaboration], these proceedings.
- [10] I. Tserruya [PHENIX Collaboration], these proceedings.
- [11] M. McCumber [PHENIX Collaboration], these proceedings.
- [12] A. Adare, *et al.* [PHENIX Collaboration], arXiv:1208.2254 [nucl-ex].
- [13] K. Aamodt *et al.* [ALICE Collaboration], Phys. Lett. B **696**, 30 (2011).
- [14] A. Adare, *et al.* [PHENIX Collaboration], arXiv:1204.1526 [nucl-ex].
- [15] E. O'Brien [PHENIX Collaboration], these proceedings.
- [16] A. Adare *et al.* [PHENIX Collaboration], Phys. Rev. Lett. **103**, 082002 (2009)